

Journal Pre-proofs

Research article

Solvation-structure-preserved electrolyte breaks the low temperature barrier for sodium metal battery

Pengbin Lai, Yaqi Zhang, Jinggang Liu, Zijian Zhang, Honghao Xie, Xinyu Li, Xiaodie Deng, Boyang Huang, Peng Zhang, Jinbao Zhao

PII: S2095-4956(25)00403-6
DOI: <https://doi.org/10.1016/j.jechem.2025.05.010>
Reference: JECHEM 4718

To appear in: *Journal of Energy Chemistry*

Received Date: 23 April 2025
Revised Date: 6 May 2025
Accepted Date: 6 May 2025

Please cite this article as: P. Lai, Y. Zhang, J. Liu, Z. Zhang, H. Xie, X. Li, X. Deng, B. Huang, P. Zhang, J. Zhao, Solvation-structure-preserved electrolyte breaks the low temperature barrier for sodium metal battery, *Journal of Energy Chemistry* (2025), doi: <https://doi.org/10.1016/j.jechem.2025.05.010>

This is a PDF file of an article that has undergone enhancements after acceptance, such as the addition of a cover page and metadata, and formatting for readability, but it is not yet the definitive version of record. This version will undergo additional copyediting, typesetting and review before it is published in its final form, but we are providing this version to give early visibility of the article. Please note that, during the production process, errors may be discovered which could affect the content, and all legal disclaimers that apply to the journal pertain.

© 2025 Published by Elsevier B.V. and Science Press on behalf of Science Press and Dalian Institute of Chemical Physics, Chinese Academy of Sciences



Solvation-structure-preserved electrolyte breaks the low temperature barrier for sodium metal battery

Pengbin Lai^{a,1}, Yaqi Zhang^{a,1}, Jinggang Liu^a, Zijian Zhang^a, Honghao Xie^a, Xinyu Li^b, Xiaodie Deng^a, Boyang Huang^c, Peng Zhang^{b,*} and Jinbao Zhao^{a,*}

^a *State-Province Joint Engineering Laboratory of Power Source Technology for New Energy Vehicle, Engineering Research Center of Electrochemical Technology, Ministry of Education, College of Chemistry and Chemical Engineering, Xiamen University, Xiamen 361005, P.R. China*

^b *College of Energy, Xiamen University, Xiamen 361102, P.R. China*

^c *Anhui Provincial Key Laboratory of Advanced Catalysis and Energy Materials, Ultra High Molecular Weight Polyethylene Fiber Engineering Research Center of Anhui Province, Anqing Normal University, Anqing 246133, P.R. China*

¹These authors contributed equally to this work.

*Corresponding authors.

E-mail addresses: pengzhang@xmu.edu.cn (P. Zhang), jbzha@xmu.edu.cn (J. Zhao).

ABSTRACT

Sodium metal batteries (SMBs) are expected to become an alternative solution for energy storage and power systems in the future due to their abundant resources, substantial energy-density, and all-climate performance. However, uneven Na deposition and slow charge transfer kinetics still significantly impair their low temperature and rate performance. Herein, we report a non-solvating trifluoromethoxy benzene (PhOCF₃) that modulates dipole-dipole interactions in the solvation structure. This modulation effectively reduces the affinity between Na⁺ and solvents, promoting an anion-rich solvation sheath formation and significantly enhancing room temperature electrochemical performance in SMBs. Furthermore, temperature-dependent spectroscopic characterizations and molecular dynamics simulations reveal that these dipole-dipole interactions thermodynamically exclude solvent molecules from inner Na⁺ solvation sphere at low temperatures, which endows the electrolyte with exceptional temperature adaptability, leading to remarkable improvement in low temperature SMB performance. Consequently, Na||Vanadium phosphate sodium (NVP) cells with the optimized electrolyte achieve 10000 cycles at 10 C with capacity retention of 90% at 25°C and over 650 cycles at 0.5 C with a capacity of 92.1 mAh g⁻¹ at -40°C. This work probed the temperature-responsive property of Na⁺ solvation structure and designed the temperature-adaptive electrolyte by regulating solvation structure via dipole-dipole interactions, offering a valuable guidance for low temperature electrolytes design for SMBs.

Keywords: Solvation structure; Sodium metal battery; Low temperature; Temperature-adaptivity; Fast charging

1. Introduction

Lithium batteries are widely used as essential energy storage devices. However, with the increasing demand for energy, the limitations of lithium resources, including their scarcity and uneven distribution, are becoming more difficult to ignore. In contrast, sodium is comparatively low-cost and widely available [1–3]. Additionally, the Stokes radius of sodium ions (4.6 Å) is smaller than that of lithium ions (4.8 Å), which grants higher ion transport capabilities and makes them particularly promising for low temperature applications [4]. Therefore, developing sodium-based batteries is a crucial complement to lithium batteries. Moreover, sodium metal as anode offers enhanced energy density with the advantage of high theoretical specific capacity (1166 mAh g⁻¹) and low reduction potential (-2.71 V vs standard hydrogen electrode). However, undesirable side reactions and redundant solid electrolyte interphase (SEI) between sodium metal anode (SMA) and conventional carbonate electrolyte lead to poor cycle performance [5–8]. In addition, low temperatures pose more obstacles to the electrolyte in aspects of slow bulk ion transport and a sluggish desolvation process at the

electrolyte/electrode interface, which undermine the performance advantages of SMBs in low temperature environments [9].

Developing suitable electrolytes is considered as a cost-effective and pragmatic approach to addressing the aforementioned challenges of Sodium metal batteries [10–12] (SMBs). Traditional carbonate-based electrolytes undergo intensive side reactions with SMA. Such severe reactions lead to uneven Na deposition and even the growth of Na dendrite, deteriorating the electrochemical performance of SMBs. What's worse, the high melting point, high viscosity and strong binding ability of carbonate solvents with Na^+ restrict their application in low temperature environments. Therefore, it is imperative to develop new electrolyte systems.

Similar to lithium electrolytes, the promising design strategies for sodium electrolytes have been extensively studied, including high-concentration electrolytes [13] (HCEs), localized high-concentration electrolytes [14,15] (LHCEs), weakly solvating electrolyte [16], and additives [17,18]. These strategies essentially take effect by adjusting the solvation structure centered on Na^+ or altering the film formation process. Consequently, the participation of free solvents in SEI chemistry is reduced, leading to a lower content of organic components that hinder ion diffusion. In other words, more anions involved in the inner solvation sheath facilitate the formation of an inorganic-rich SEI layer, which exhibits high ionic conductivity, enhanced mechanical strength and increased interfacial energy, thereby suppressing the growth of Na dendrites [19].

Drawing from the foregoing analysis, an ideal electrolyte for SMBs needs to satisfy the following requirements [20,21]: (1) wide liquid range and excellent ionic conductivity in the bulk electrolyte. (2) good chemical and electrochemical stability with both the cathode and anode. (3) rapid desolvation process during electrochemical cycling, which usually is the rate-determining step at low temperature working condition. (4) ability to ensure the reversible intercalation/deintercalation process of cathode material and uniform plating/stripping of SMA. Besides, it is noteworthy that recent works have demonstrated that temperature variations exert a significant impact on the solvation structure. At reduced temperatures, the combined effects of solvent molecule contraction and enhanced intermolecular interactions lead to a disproportionately increased growth rate of cation-solvent interactions relative to cation-anion interactions, thereby driving solvent molecules into the inner solvation shell. This thermodynamic preference, arising from both volumetric contraction and strengthened interaction forces at low temperatures, induces a pronounced shift in solvation structure, characterized by an increased population of solvent-separated ion pair (SSIP) at the expense of contact ion pair (CIP) and aggregate (AGG) species [22,23]. This unfavorable temperature-dependent evolution of solvation structures leads to slower desolvation kinetics and inferior interfacial chemistry at low temperatures, thereby deteriorating the cell's electrochemical performance. Apart from lithium electrolyte, this temperature-responsive characteristic of solvation structure also manifests in sodium electrolyte [24,25]. Therefore, the temperature adaptability of the

solvation structure should also be considered during the design of low temperature sodium electrolytes.

In this work, a low melting-point and low-polarity linear carboxylate ester, methyl propionate (MP), serves as the primary solvent. And fluoroethylene carbonate (FEC) is used in combination to improve the chemical and electrochemical compatibility with SMA. Besides, the trifluoromethoxy benzene (PhOCF₃) diluent was introduced to increase the proportion of anion in inner Na⁺ solvation structure owing to its non-solvating property and dipole-dipole interactions with other solvents (Fig. 1). This behavior facilitates the anion-derived solvation structure and promotes the formation of an inorganic-rich SEI, which is beneficial for improving the cycling performance of SMBs. Furthermore, temperature-dependent theoretical calculations and spectroscopic characterizations reveal that the optimized electrolyte display the preservation of the solvation structure, enabling smooth Na deposit and stable cycle performance at low temperatures. As a result, Na||NVP cells utilizing the MFP electrolyte (1 M NaPF₆ in MP/FEC/PhOCF₃, 1:1:1 by volume) demonstrate excellent high-rate and low temperature performance compared to MF11 (1 M NaPF₆ in MP/FEC, 1:1 by volume) and PE11 (1 M NaPF₆ in PC/EMC, 1:1 by volume) electrolytes. This work systematically investigated the temperature-responsive characteristics of the solvation structure in sodium electrolytes. By capitalizing on the dipole-dipole interactions between PhOCF₃ and solvents, adverse effects at low temperatures were effectively mitigated. These findings offer fundamental guidelines for engineering temperature-resilient sodium electrolytes, paving the way for reliable sodium battery operation under low temperature conditions.

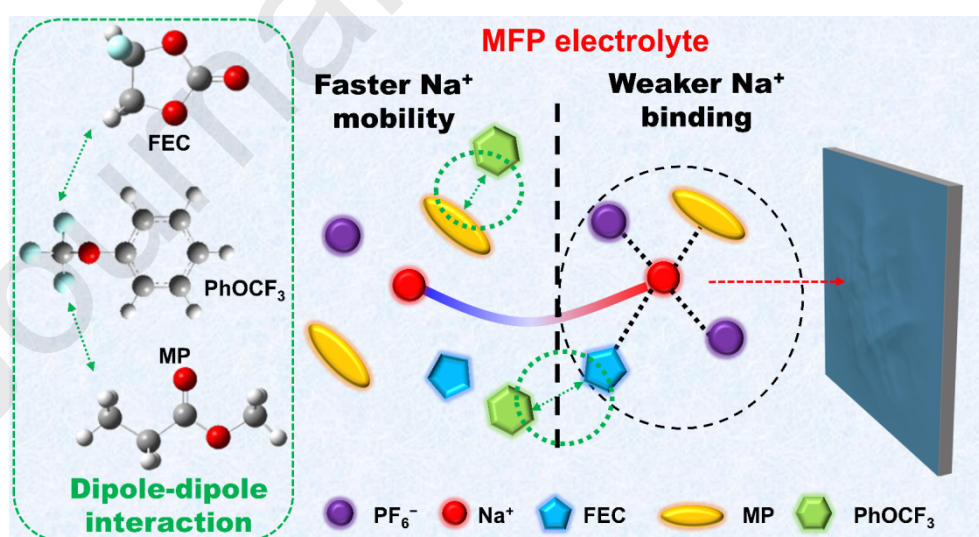


Fig. 1. Schematic illustration of Na⁺ transportation and interfacial chemistry in MFP electrolyte.

2. Results and discussion

2.1. Evaluation of the solvation structure of electrolytes

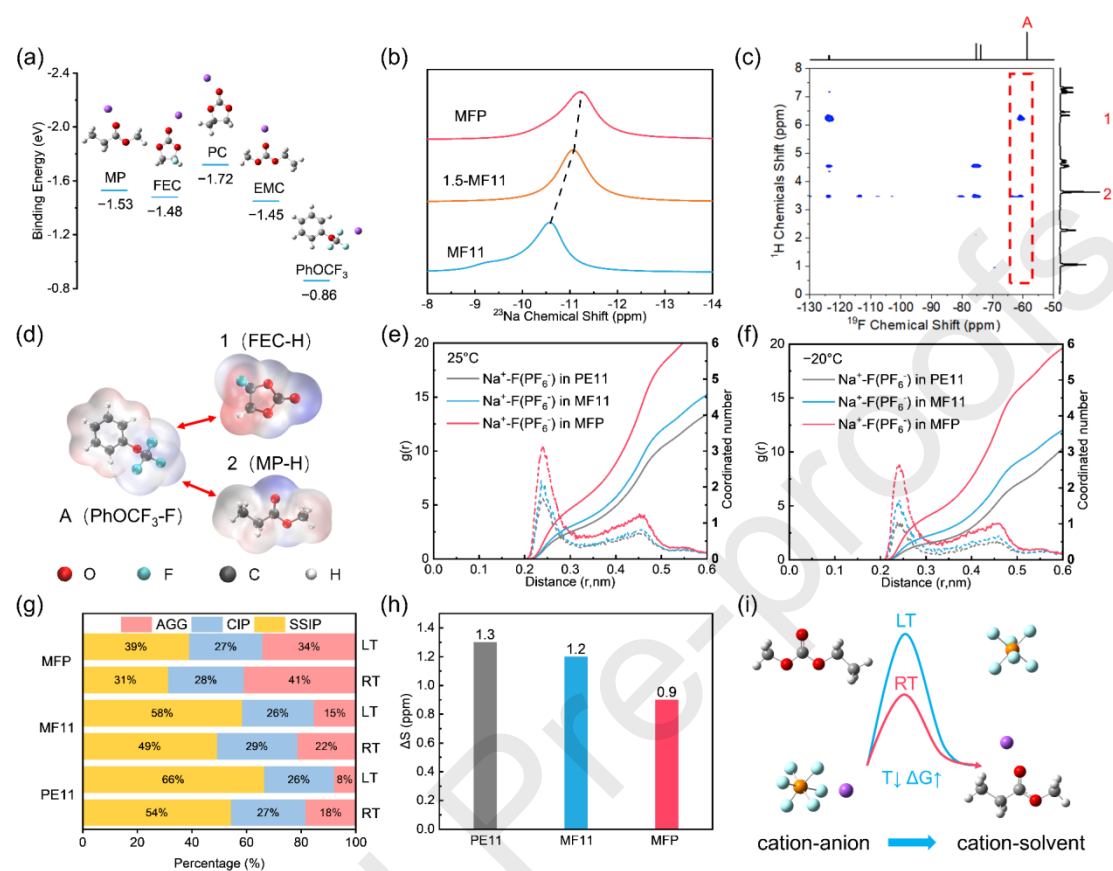


Fig. 2. (a) The binding energy of solvent with Na⁺. (b) ²³Na NMR spectra of electrolytes. (c) ¹H-¹⁹F HOESY of MFP electrolyte. (d) Schematic diagram of the interactions of PhOCF₃ with MP and FEC. (e) Radial distribution function (RDF, *g(r)*) and coordinated number (CN) of PF₆⁻ for three electrolytes at 25°C and (f) at -20°C. (g) The solvation structure distribution analysis of the three electrolytes at room and low temperatures. (h) The chemical shift offset of ²³Na spectra between room temperature and low temperature in three electrolytes. (i) Illustration of solvent molecule replacing the anion of the solvation structure at room and low temperatures.

The binding energy serves as a crucial indicator for assessing the coordination ability of solvents and the calculated results are as shown in Fig. 2(a). Among these solvents, the binding affinity of PhOCF₃ with Na⁺ (-0.86 eV) is significantly weaker than that of other solvents, indicating that PhOCF₃ has limited participation in the inner solvation of Na⁺ in comparison with other solvents. This result is also corresponded to the electrostatic potential (ESP) result in Fig. S1. It is worth noting that, due to the limited solubility of PhOCF₃ for the salt of NaPF₆ (as shown in Fig. S2), the actual concentration of the MFP electrolyte is closer to 1.5 M rather than 1.0 M. To eliminate

the influence of the concentration effect on the solvation structure, we compared the differences in the solvation structures of MFP and the electrolyte with an equivalent concentration of MF11 (1.5-MF11, 1 M NaPF₆ in MP/FEC, 1:1 by volume). To discern the coordination state, ²³Na NMR tests were performed on the electrolytes, and the results are shown in Fig. 2(b). The chemical shift of ²³Na nuclei in 1.5-MF11 is more negative than that in MF11. This stems from an increased number of anions coordinating with Na⁺, which enhances the shielding effect. Additionally, the ²³Na nuclei in MFP exhibit an even more negative chemical shift than those in 1.5-MF11, indicating that there are some additional interactions driving more anions into the inner solvation sheath. Therefore, heteronuclear Overhauser effect spectroscopy (HOESY), a type of two-dimensional NMR, was conducted to analyze the interactions among solvent molecules. The signals enclosed by the dotted-line box in ¹H-¹⁹F HOESY indicate the solvent-solvent interaction between PhOCF₃ and cosolvents (Fig. 2c). The Fig. 2(d) visually represents the intermolecular interactions between the electronegative fluorine (F atom of PhOCF₃) and electropositive hydrogen (H atom of MP and FEC). As a result, the electronic density of the F atom decreases, while that of the H atom increases accordingly (Fig. S3). The formation of PhOCF₃-MP and PhOCF₃-FEC complexes contributes to altering the solvent coordination.

To obtain the detailed information of solvation structure, MD simulations were conducted to analyze $g(r)$ and CN of Na⁺, as shown in Fig. S4. In the MFP electrolyte, a distinct solvent peak appears around 3.0 Å with a high CN, while there is no notable peak of PhOCF₃, indicating its absence in the inner layer. The Fig. 2(e) and Table S1 compares the CN of Na⁺ with PF₆⁻ increases from 0.89 in MF11 to 1.37 in MFP. Both of them are significantly higher than that in the conventional carbonate electrolyte PE11 (0.73). Based on this, it can be inferred that the introduction of PhOCF₃ not only reduces the number of coordinating solvents but also impairs their binding strength through dipole-dipole interactions, facilitating more anions to approach inner solvation structure [26–28]. It is worth-noting that the CN of anions in MFP is higher than that of 1.5-MF11 electrolyte, confirming the effect of dipole-dipole interactions (Fig. S5).

When the simulation temperature is decreased from 298 K to 253 K (Fig. 2f and Fig. S6), the CN of PF₆⁻ in all electrolytes decreases to 0.44 (PE11), 0.64 (MF11), and 1.17 (MFP), aligning with conclusions from previous work [29]. And it can be seemed in Fig. 2(g) and Table S2-S7 that the proportion of CIP and AGG in MFP electrolyte is higher those in MF11 and PE11 at room and low temperatures, suggesting its good temperature-adaptivity. The results of MD simulation are corroborated by the temperature-dependent NMR results. In Fig. S7, the chemical shift of ²³Na peak in MFP increases from -12.2 ppm at room temperature to -11.3 ppm at -20°C, suggesting a reduction in the surrounding anions. In comparison, the peak position for MF11 rises from -11.8 ppm to -10.6 ppm, while for PE11 it increases from -11.4 ppm to -10.1 ppm. The peak displacements ΔS in the two electrolytes are both greater than that in MFP (Fig. 2h). This trend is also observed in ¹⁹F and ³¹P spectra (Figs. S8 and S9). Apart from that, in the temperature-dependent Raman result, the P-F vibrational peak [30] (Fig. S10) around 745 cm⁻¹ shifts to lower wavenumbers with decreasing

temperature, and the variation in MFP electrolyte is less than that in the MF11 electrolyte (Fig. S11), indicating that the introduction of PhOCF₃ can suppress the changes in solvation structure with temperature. The temperature-dependent spectral results further illustrate that the solvation structure of MFP exhibits good preservations against temperature changes, which is advantageous for leveraging the benefits of the solvation structure at low temperatures, thereby improving the cell's low temperature performance.

To further validate this change, density functional theory (DFT) methods were carried out to calculate the Gibbs energy (ΔG) required to substitute anions with solvent molecules at different temperatures, as illustrated in Fig. 2(i). Taking EMC as an example, at room temperature (298 K), substituting a PF₆⁻ with EMC and coordinating with Na⁺ requires overcoming an energy of 0.64 kcal mol⁻¹, while at 253 K, the Gibbs energy drops to 0.52 kcal mol⁻¹, indicating that solvent substitution for anions is easier at lower temperatures. A series of calculations for various solvents is presented in Fig. S12. Regardless of temperature, the Gibbs energies for MP and FEC solvents are higher than those for other solvents, suggesting that it is harder for these two solvents to enter the inner solvation structure to replace anions. As for MFP electrolyte, due to the dipole-dipole interactions between PhOCF₃ and other solvents, the solvent molecules will be dragged out of Na⁺ inner solvation structure while the anions remain in the inner solvation layer. This phenomenon renders solvent substitution necessitate the overcoming of significantly higher energy barriers, thereby exacerbating the difficulty of this process. These results above demonstrate the order of temperature-response sensitivity of solvation structures in three electrolytes: PE11 > MF11 > MFP, indicating that the MFP electrolyte is less affected by temperature, maintaining the advantage of favorable solvation structures at various temperatures. It is worth noting that the dipole-dipole interactions also have an inhibitory effect on unfavorable variations of the solvation structure at low temperatures. Detailed discussions can be found in Fig. S13.

2.2. Analysis of ion transportation in the bulk electrolyte and at the interface

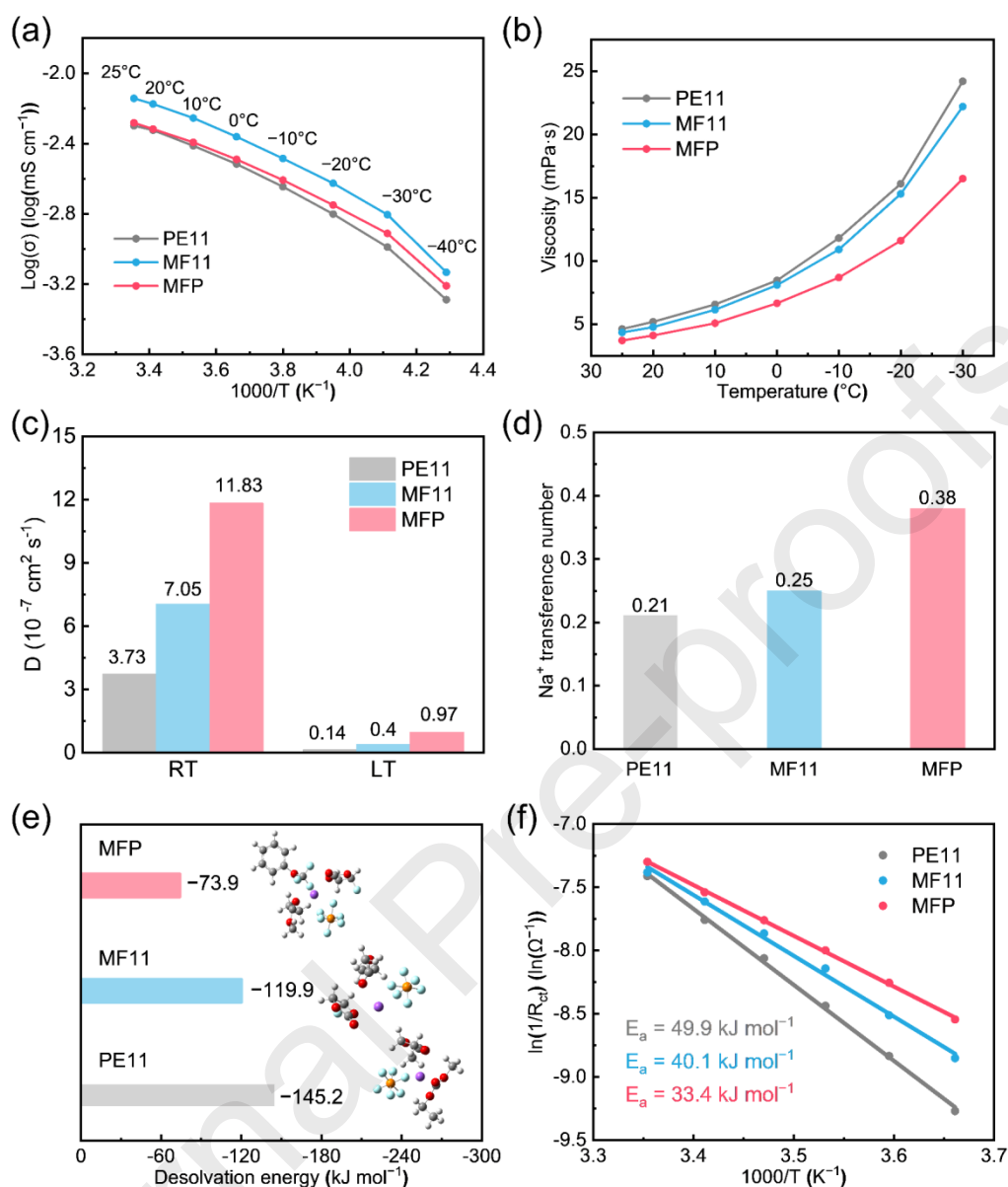


Fig. 3. (a) The conductivity of three electrolytes at different temperatures. (b) The viscosity of three electrolytes at different temperatures. (c) The calculated MSD of electrolytes at room and low temperatures. (d) Na^+ transference number (t_{Na^+}) of electrolytes. (e) Calculated solvation energy in three electrolytes ($\text{Na}^+\text{-PF}_6^-$ -MP-FEC- PhOCF_3 for MFP electrolyte; $\text{Na}^+\text{-PF}_6^-$ -MP-FEC for MF11 electrolyte; $\text{Na}^+\text{-PF}_6^-$ -PC-EMC for PE11 electrolyte). (f) Calculated E_a of Na^+ charge transfer process in three electrolytes.

Conductivity and viscosity are important indicators for evaluating the transport of ions (Fig. 3a, b). It can be observed that the conductivity of MFP is lower than that of MF11 at both room temperature and low temperatures, which is due to the addition of the low dielectric constant PhOCF_3 . Despite this, the conductivity of MFP remains

slightly higher than that of the carbonate electrolyte. As for the viscosity, all electrolytes exhibit exponential growth in viscosity at low temperatures, while the addition of PhOCF_3 could mitigate this rapid increase. Furthermore, the contact angle between the MFP electrolyte and the PE separator (20.4°) is significantly lower than that of MF11 (41.0°) and PE11 (41.5°), indicating good wettability of MFP with the separator (Fig. S14). The transportation of Na^+ in the bulk electrolyte can be determined by tracking the mean square displacement (MSD). As shown in Fig. 3(c), the calculated diffusion coefficient of MFP electrolyte is the highest in both room and low temperatures (Fig. S15 and Table S8). Additionally, the transference number of the MFP electrolyte reaches 0.32, surpassing that of MF11 and PE11 (Fig. 3d and Fig. S16). Beyond bulk diffusion, transportation at the electrode/electrolyte interface especially the desolvation process, is a critical factor influencing cell's electrochemical performance at low temperatures [31]. The solvation energy of MFP obtained by DFT calculation is the lowest among the three electrolytes, facilitating a faster desolvation process at the interface (Fig. 3e). To quantitatively investigate the kinetics of the desolvation process, temperature-dependent EIS testing was employed. As shown in Fig. 3(f) and Fig. S17, the activation energy (E_a) for the PE11 electrolyte is 49.9 kJ mol^{-1} , stemming from the strong interaction between Na^+ and EMC/PC solvents. In the MF11 electrolyte, the E_a value decreases to 40.1 kJ mol^{-1} . Following the addition of the PhOCF_3 , the E_a value further reduces to 33.4 kJ mol^{-1} , indicating a faster charge transfer process at the interface. This is corroborated by the Tafel plots at room and low temperatures (Fig. S18).

2.3. Compatibility with Na metal anode

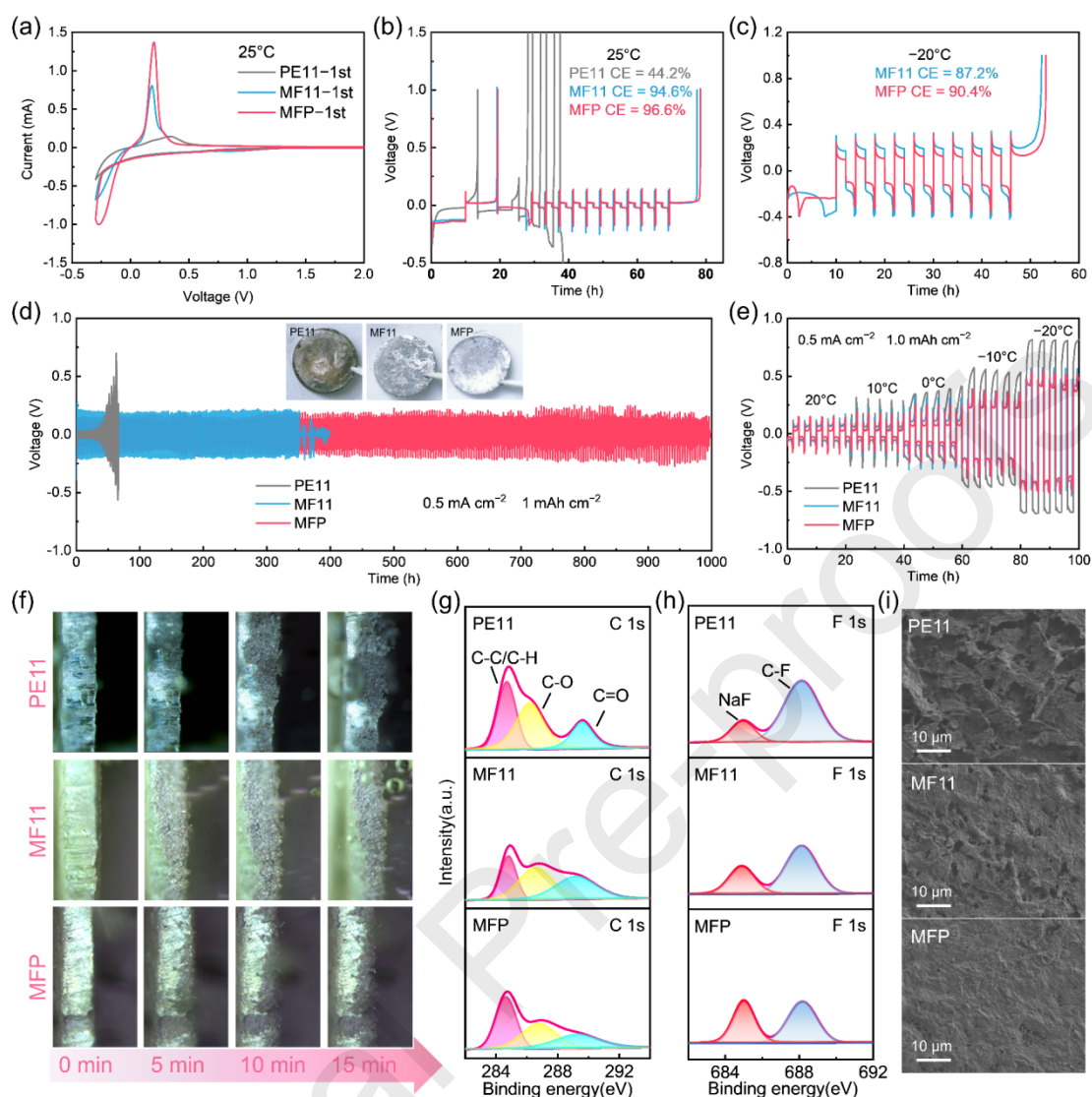


Fig. 4. (a) The CV tests of Na||Al cells scanned between -0.3 and 2.0 V at 1 mV s^{-1} at 25°C . The CE of Na||Al cells at (b) 25°C and at (c) -20°C . (d) The voltage profile of Na||Na symmetric cells in three electrolytes; insert is the morphology of cycled Na metals. (e) The voltage profile of Na||Na symmetric cells in three electrolytes at different temperatures. (f) The in situ deposition process of SMA with different electrolytes. The (g) C $1s$ and (h) F $1s$ XPS profiles of cycled SMA with three electrolytes. (i) The morphology of cycled SMA in Na||Na symmetric cells with three electrolytes.

To investigate the chemical stability of carboxylic esters with SMA, the changes of SMA after contacting with various solvents for a period was firstly observed. As shown in Fig. S19, pure MP solvent turned yellow after being in contact with SMA for 5 days, indicating the presence of side reactions [32]. However, upon the addition of FEC and PhOCF_3 as co-solvents, this side reaction was suppressed, indicating that these two fluorinated solvents can inhibit the side chemical reactions between carboxylic

esters and SMA, thus enhancing their chemical stability.

In addition to chemical stability, the electrochemical stability of the three electrolytes was also assessed through cyclic voltammetry (CV) test. As shown in Fig. 4(a) and Fig. S20, the MFP electrolyte exhibits a strong peak at -0.3 V during the negative sweep, corresponding to the deposition of Na on aluminum. In contrast, the peaks for MF11 and PE11 are relatively weak, indicating poorer deposition reversibility. Furthermore, the reversibility of Na plating/stripping can be evaluated using Na||Al cells. As illustrated in Fig. 4(b), the cells using MFP electrolyte achieve a high Coulombic efficiency (CE) of 96.6%, surpassing those with PE11 and MF11, demonstrating that this electrolyte possesses electrochemical stability favorable for reversible Na deposition. Additionally, at -20°C , the MFP electrolyte still attains a higher CE of 90.4%, attributable to its ability to preserve a solvent structure rich in anions, while MF11 reaches only 87.2% (Fig. 4c). To verify the stability of the plating/stripping process, long-cycle tests were conducted using sodium symmetric cells, as shown in Fig. 4(d). In PE11 electrolyte, voltage hysteresis begins to increase after a few cycles, reaching over 0.5 V within 80 h, while the MF11 electrolyte exhibits short-circuiting after 350 h, both of which can be attributed to their unstable SEI [33]. In contrast, the MFP electrolyte demonstrates relatively small polarization, maintaining stable cycling for 1000 h, indicating good compatibility with SMA. Even when the cycling rate increases to 5 mAh cm^{-2} , the cells in MFP electrolyte still exhibit smallest polarization among three electrolytes (Fig. S21). Moreover, at different temperatures, Na||Na symmetric cells using the MFP electrolyte exhibit the least polarization, highlighting its good temperature adaptability (Fig. 4e). Therefore, the MFP electrolyte outperforms the other electrolytes in both chemical and electrochemical stability, maintaining its advantages even at low temperatures.

Then, in situ optical microscopy was employed to observe the dynamic deposition process of transparent quartz Na||Na symmetric cells. As shown in Fig. 4(f), after 15 min of deposition, the SEI formed in PE11 electrolyte fails to adequately protect the SMA, resulting in a significant amount of heterogeneous Na dendrite plating and numerous gas bubbles. The interface in MF11 shows reduced dendrite growth and bubble formation, yet still remain a considerable number of Na dendrites. In the MFP electrolyte, the presence of Na dendrites is further minimized, indicating that the formed SEI promotes more uniform Na deposition and effectively suppresses dendrite growth.

The chemical composition of the SEI formed in different electrolytes was analyzed using X-ray photoelectron spectroscopy (XPS). Fig. 4(g, h) exhibit the C 1s and F 1s spectra of the SMA surface after cycling, respectively. The C 1s spectra for all three electrolytes can be divided into C-C (284.8 eV), C-O (286.7 eV), and C=O (289.8 eV) components, primarily resulting from solvent decomposition, which is detrimental to the protection of the SMA [34,35]. Notably, the intensity of the C peak for the PE11 electrolyte is greater than those of other electrolytes, indicating that its SEI is solvent-derived. Furthermore, the O 1s spectrum (Fig. S22) reveals that the SEI formed in the

PE11 electrolyte shows strong signals for Na_2CO_3 and C-O peaks, which cannot effectively suppress side reactions, leading to the degradation of the electrochemical performance [36]. In contrast, the MFP electrolyte exhibits relatively weaker intensities for these components. Additionally, the F spectrum shows a strong NaF signal, which may be attributed to the preferential adsorption of PhOCF_3 (Fig. S23 and S24) and the anion-rich solvation structure of MFP electrolyte. This inorganic component can suppress side reactions, reduce electrolyte consumption and facilitate uniform Na deposition [37].

The surface morphology of cycled SMA in different electrolytes was observed using scanning electron microscopy (SEM), as shown in Fig. 4(i) and Fig. S25. In the PE11 electrolyte, a loose and porous morphology is observed on the surface of SMA, which is detrimental to stable cycling of the batteries. Although the MF11 electrolyte exhibits a generally smooth surface, some holes and Na dendrites are still present. In contrast, the electrodes cycled in the MFP electrolyte are flat and uniform, indicating the formation of a homogeneous and inorganic-rich SEI that is beneficial for suppressing dendrite growth and enabling reversible Na deposition.

2.4. Electrochemical performance and interphase properties of Na||NVP cells

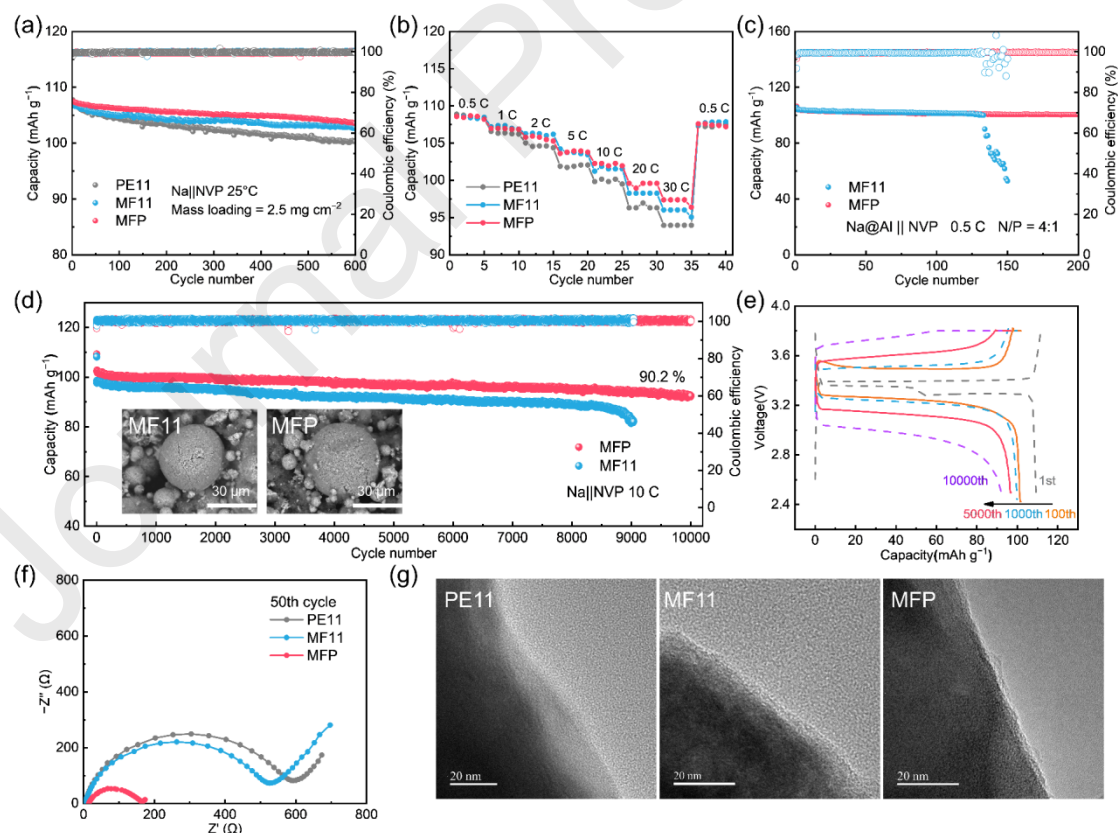


Fig. 5. (a) The cycling performance of low-loading Na||NVP cells at room temperatures at 1 C rate. (b) The rate performance of Na||NVP cells in three electrolytes from 0.5 C

to 30 C. (c) The cycling performance of Na@Al||NVP full cells using MFP electrolytes with N/P ratio of 4:1. (d) The cycling performance of Na||NVP cells using MFP electrolyte at 10 C. Inset is the SEM image of cycled NVP particle in MF11 and MFP electrolytes. (e) The corresponding voltage profiles of cells at different cycles. (f) TEM images of CEI after 100 cycles in three electrolytes. (g) The Nyquist plots of cycled Na||NVP cells in three electrolytes.

The electrochemical windows of three electrolytes were determined using linear sweep voltammetry (LSV), as shown in Fig. S26. Both MF11 and MFP electrolytes exhibit excellent oxidative stability, indicating that the designed carboxylic ester electrolytes are compatible with the NVP cathode material. Subsequently, Na||NVP cells were assembled and tested with the three electrolytes (Fig. 5a). Under low loading conditions (2.5 mg cm^{-2}), the capacity retention rates at a 1 C rate are comparable for three electrolytes, with the MFP electrolyte (96.4%) slightly outperforming the other two reference samples (MF11 at 95.8% and PE11 at 93.0%). However, as the mass loading increased to 9 mg cm^{-2} , the performance difference among electrolytes began to manifest. As shown in Fig. S27, the Na||NVP cells using the MFP electrolyte maintains a high capacity retention of 88.6% after 1000 cycles at 1 C, outperforming the MF11 electrolyte (83.0%). In contrast, the PE11 electrolyte exhibits a significant capacity decline, with less than 3.0 mAh g^{-1} remaining after 200 cycles, likely due to its poor SMA compatibility and slower desolvation process. Besides, the MFP electrolyte also demonstrates better rate performance. As shown in Fig. 5(b), the cells in MFP electrolyte can maintain a capacity retention rate as high as 89.8% at a rate of 30 C.

Given the excellent electrochemical performance of MF11 and MFP, we assembled Na||NVP full cells for testing, with the anode consisting of limited Na deposition on aluminum foil (Na@Al) and high-loading cathode NVP, resulting in a final N/P ratio of 4:1. As shown in Fig. 5(c), the Na@Al||NVP cells in MFP electrolyte exhibit an average CE of 99.6% over more than 200 cycles, with a capacity retention of 94.4%. This is primarily attributed to the anion-derived inorganic SEI formed by MFP, as well as its enhanced interfacial ionic transport characteristics. Additionally, Na||NVP cells with MFP electrolyte can stably cycle at a high rate of 10 C for 10000 cycles, achieving a high capacity retention of 90.2% (Fig. 5d, e and Table S9). In contrast, the cells in PE11 only maintain 58.2% capacity after 5000 cycles (Fig. S28).

The outstanding high-rate performance is largely due to the stable and reversible SEI formed after the addition of PhOCF_3 . The inset SEM images demonstrate that the cycled NVP particle in MFP electrolyte remains relatively complete compared with that in PE11 (Fig. S29), suggesting that the optimized electrolyte plays a good role in protecting cathode during high-rate cycling. Furthermore, Nyquist plots of Na||NVP cells using different electrolytes at different cycles indicate that MFP electrolyte demonstrates lower impedance value, consistent with its stable electrochemical

performance (Fig. 5f).

In order to further reveal the mechanism of different electrolytes on the surface of the cathode, TEM was carried out to observe the cathode material after high-rate cycling, and the results are shown in Fig. 5(g). It can be found that after high-rate cycling, the CEI formed in PE11 electrolyte is quite thick and uneven, which is detrimental to Na^+ transport. In contrast, the CEI in MFP electrolyte is relatively thinner and uniform, indicating that MFP can facilitate the formation of a stable interface during cycling, as corroborated by in situ impedance tests (Fig. S30). Apart from that, the chemical component of CEI formed in three electrolytes is also analyzed with XPS characterization (Fig. S31). The CEI in MFP possesses higher proportion of inorganic component like NaF and less organic component, which could protect cathode from side reaction [38].

2.5. Low temperature electrochemical performance

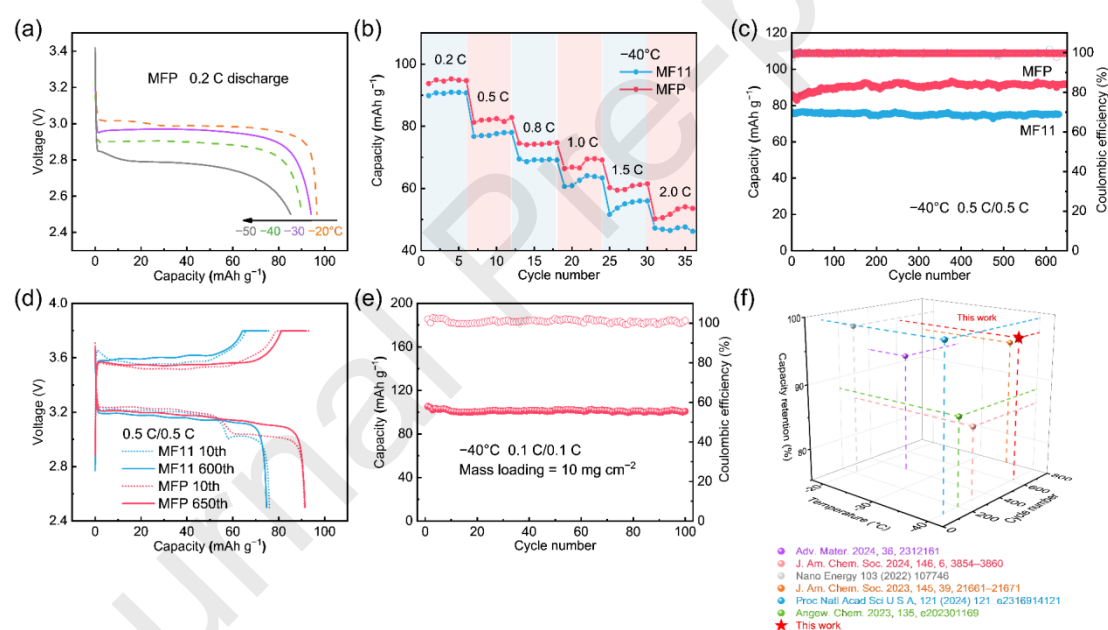


Fig. 6. (a) The discharge performance of three electrolytes at various temperatures. (b) The rate performance of MF11 and MFP electrolytes at -40°C . (c) The cycling performance and (d) charge/discharge profiles of low-loading Na||NVP cells at 0.5 C at -40°C . (e) The cycling performance of high-loading Na||NVP cells at 0.1 C at -40°C . (f) Comparative performance of Na||NVP cells at low temperatures in this work with those of previous literature (detail comparison can be seen in Table S10).

The discharge performance of Na||NVP cells with MFP electrolyte at different low temperatures under a discharge rate of 0.2 C is shown in Fig. 6(a). At -20°C , their discharge capacities are similar, all exceeding 90 mAh g^{-1} . However, as the temperature

further decreases, the capacities of Na||NVP cells with PE11 and MF11 electrolytes significantly decline, with discharge capacity of only 29.1 and 66.0 mAh g⁻¹ at -50°C, respectively (Fig. S32). In contrast, the MFP electrolyte retains a capacity of 85.2 mAh g⁻¹ at -50°C, primarily due to its low viscosity and improved ionic transportation. This excellent discharge performance corresponds to previous results from temperature-dependent viscosity and MSD calculations. In addition to excellent discharge performance, the MFP electrolyte also demonstrates superior high rate performance, achieving a high capacity of 53.5 mAh g⁻¹ at -40°C at 2 C rate (Fig. 6b), whereas PE11 exhibits nearly no capacity (Fig. S33).

In terms of long-term cycling performance, as shown in Fig. 6(c, d), the low-loading Na||NVP cells using the MFP electrolyte maintain a capacity of 92.1 mAh g⁻¹ after 650 cycles at -40°C under a rate of 0.5 C, which is higher than the 75.1 mAh g⁻¹ capacity of MF11 after 600 cycles. Although the PE11 electrolyte remains liquid at -40°C, it does not work at this temperature, which is likely due to its higher desolvation energy barrier and the formation of a poor SEI (Figs. S34 and S35). Furthermore, under high loading and limited sodium conditions, the optimized MFP electrolyte continues to perform at -40°C, maintaining a capacity of 100.8 mAh g⁻¹ after 100 cycles at 0.1 C, indicating its practical application (Fig. 6e). The low temperature electrochemical performance of the Na||NVP cells is compared with other works (Fig. 6f and Table S10). Obviously, the MFP electrolyte designed in this work exhibits exceptional low temperature, high-rate and long-cycling performance.

3. Conclusions

In summary, this work introduced non-solvating PhOCF₃ into the carboxylate-based electrolyte. The results of two-dimensional NMR indicate that there are the dipole-dipole interactions between PhOCF₃ and solvents, which can weaken the affinity of Na⁺-solvent and promote the formation of an anion-rich solvation structure. This kind of solvation structure could improve the chemical and electrochemical stability of the interface by forming inorganic-rich SEI, therefore promoting uniform and reversible Na deposition with a homogeneous morphology and thus improving the room temperature electrochemical performance of SMBs. In addition, it is worth mentioning that although the magnitude of the dipole-dipole interactions is relatively small at room temperature, their growth rate is much higher than that of the cation-solvent and cation-anion interactions as the temperature decreases. This property enables MFP to preserve an anion-rich solvation structure even at low temperatures, which is beneficial for preserving the designed solvation structure thus enhancing the electrochemical performance of SMBs at low temperatures. With these benefits, the optimized MFP electrolyte not only demonstrates a capacity retention of 90.2% after 10000 stable cycles at a high rate of 10 C at room temperature, but also maintains a retention of 97.0% after 650 cycles at -40°C. This work puts forward a method to inhibit the unfavorable variation of solvation structures at low temperatures via dipole-

dipole interactions between PhOCF₃ and solvents, providing a new perspective on the design of low temperature sodium electrolytes.

Experimental section

Experimental details can be found in Supporting Information.

Data Availability

The data are available on request from the corresponding author.

Declaration of Competing Interest

The authors declare no competing financial interest.

Acknowledgements

We gratefully acknowledge the financial support of National Key Research and Development Program of China (2021YFB2400300), National Natural Science Foundation of China (21875198,21875195), the Fundamental Research Funds for the Central Universities (20720190040) and the key Project of Science and Technology of Xiamen (3502Z20201013). And we are grateful to Tan Kah Kee Innovation Laboratory (IKKEM) for help with XPS, SEM, NMR and Raman measurements. The numerical calculations in this paper have been done on Hefei advanced computing center.

Appendix A. Supplementary data

Supplementary data to this article can be found at Supporting Information.

References

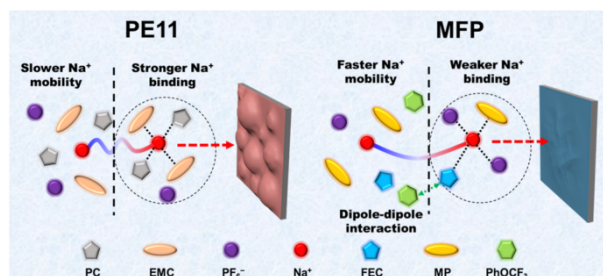
- [1] M. Armand, J.-M. Tarascon., *Nature* 451 (2008) 652–657.
- [2] P.K. Nayak, L. Yang, W. Brehm, P. Adelhelm, *Angew. Chem. Int. Ed. Engl.* 57 (2018) 102–120.
- [3] X. Wang, Y. Wu, Y. Zhou, W. Zheng, K. Zhang, X. Ma, T. Bai, D. Li, L. Ci, C.P. Grey, J. Lu, *Adv. Funct. Mater.* 35 (2024) 2414041.
- [4] K. Xu, *Chem. Rev.* 104 (2004) 4303–4417.

- [5] X. Liu, X. Zheng, Y. Dai, W. Wu, Y. Huang, H. Fu, Y. Huang, W. Luo, *Adv. Funct. Mater.* 31 (2021) 2103522.
- [6] X. Wang, J. Lu, Y. Wu, W. Zheng, H. Zhang, T. Bai, H. Liu, D. Li, L. Ci, *Adv. Mater.* 36 (2024) e2311256.
- [7] Y. Wang, Y. Wang, Y.-X. Wang, X. Feng, W. Chen, X. Ai, H. Yang, Y. Cao, *Chem* 5 (2019) 2547–2570.
- [8] J. Zhang, J. Li, G. Jia, H. Wang, M. Wang, *J. Energy Chem* 102 (2025) 340–352.
- [9] Z. Huang, Z. Xiao, R. Jin, Z. Li, C. Shu, R. Shi, X. Wang, Z. Tang, W. Tang, Y. Wu, *Energy Environ. Sci.* 17 (2024) 5365–5386.
- [10] Y. Li, F. Wu, Y. Li, M. Liu, X. Feng, Y. Bai, C. Wu, *Chem. Soc. Rev.* 51 (2022) 4484–4536.
- [11] J. Liu, Z. Ni, C. Wei, Z. Wang, S. Liu, H. Zhang, C. Yang, S. Xiong, J. Feng, *Energy Storage Mater.* 72 (2024) 103753.
- [12] M. Ma, B. Chen, X. Yang, Y. Liu, S. Dai, X. Qi, Y.-S. Hu, H. Pan, *ACS Energy Lett.* 8 (2022) 477–485.
- [13] R. Cao, K. Mishra, X. Li, J. Qian, M.H. Engelhard, M.E. Bowden, K.S. Han, K.T. Mueller, W.A. Henderson, J.-G. Zhang, *Nano Energy* 30 (2016) 825–830.
- [14] P. Lai, Y. Zhang, J. Wang, M. chen, X. Li, X. Deng, Q. Chen, B. Huang, C. Gan, Y. Zou, Y. Qiao, P. Zhang, J. Zhao, *eScience* 5 (2025) 100399.
- [15] J. Zheng, S. Chen, W. Zhao, J. Song, M.H. Engelhard, J.-G. Zhang, *ACS Energy Lett.* 3 (2018) 315–321.
- [16] S. Wang, X.G. Zhang, Y. Gu, S. Tang, Y. Fu, *J. Am. Chem. Soc.* 146 (2024) 3854–3860.
- [17] J. Shi, L. Ding, Y. Wan, L. Mi, L. Chen, D. Yang, Y. Hu, W. Chen, *J. Energy Chem* 57 (2021) 650–655.
- [18] S. Wan, K. Song, J. Chen, S. Zhao, W. Ma, W. Chen, S. Chen, *J. Am. Chem. Soc.* 145 (2023) 21661–21671.
- [19] C. Zhu, D. Wu, Z. Wang, H. Wang, J. Liu, K. Guo, Q. Liu, J. Ma, *Adv. Funct. Mater.* 34 (2023) 2214195.
- [20] Y. Yang, W. Yang, H. Yang, H. Zhou, *eScience* 3 (2023) 100170.
- [21] N. Zhang, T. Deng, S. Zhang, C. Wang, L. Chen, C. Wang, X. Fan, *Adv Mater.* 34 (2021) e2107899.
- [22] Y. Chae, C. Lim, J. Jeon, M. Kim, K.-K. Lee, K. Kwak, M. Cho, *J. Phys. Chem. Lett.* 13 (2022) 7881–7888.

- [23] Y. Mo, G. Liu, J. Chen, X. Zhu, Y. Peng, Y. Wang, C. Wang, X. Dong, Y. Xia, *Energy Environ. Sci.* 17 (2024) 227–237.
- [24] Y. Cui, Y. Ni, Y. Wang, L. Wang, W. Yang, S. Wu, W. Xie, K. Zhang, Z. Yan, J. Chen, *Adv. Energy Mater.* 15 (2025) 2405363.
- [25] Z. Huang, Z. Xiao, H. Zhang, Q. Zhang, J. Cui, J. Luo, W. Tang, Y. Wu, *J. Am. Chem. Soc.* 147 (2025) 5162–5171.
- [26] H. Liang, Z. Ma, Y. Wang, F. Zhao, Z. Cao, L. Cavallo, Q. Li, J. Ming, *ACS Nano* 17 (2023) 18062–18073.
- [27] Q. Sun, Z. Cao, Z. Ma, J. Zhang, H. Cheng, X. Guo, G.-T. Park, Q. Li, E. Xie, L. Cavallo, Y.-K. Sun, J. Ming, *ACS Energy Lett.* 7 (2022) 3545–3556.
- [28] Y. Wang, Z. Cao, Z. Ma, G. Liu, H. Cheng, Y. Zou, L. Cavallo, Q. Li, J. Ming, *ACS Energy Lett.* 8 (2023) 1477–1484.
- [29] P. Lai, Y. Zhang, B. Huang, X. Deng, H. Hua, Q. Chen, S. Zhao, J. Dai, P. Zhang, J. Zhao, *Energy Storage Mater.* 67 (2024) 103314.
- [30] L. Zhou, Z. Cao, W. Wahyudi, J. Zhang, J.-Y. Hwang, Y. Cheng, L. Wang, L. Cavallo, T. Anthopoulos, Y.-K. Sun, H.N. Alshareef, J. Ming, *ACS Energy Lett.* 5 (2020) 766–776.
- [31] Q. Li, D. Lu, J. Zheng, S. Jiao, L. Luo, C.M. Wang, K. Xu, J.G. Zhang, W. Xu, *ACS Appl. Mater. Interfaces* 9 (2017) 42761–42768.
- [32] Y. Yang, L.G. Yu, Y.X. Huang, X.Q. Ding, Z.Q. Xue, Z. Li, Y.X. Yao, S. Zhang, L. Xu, X.F. Wen, J. Pei, C. Yan, J.Q. Huang, *Angew. Chem. Int. Ed.* 64 (2025) e202503616.
- [33] X. Liu, X. Zheng, X. Qin, Y. Deng, Y. Dai, T. Zhao, Z. Wang, H. Yang, W. Luo, *Nano Energy* 103 (2022) 107746.
- [34] Y. Wang, H. Yang, J. Xu, P. Tang, Q. Wei, T. Hu, X. Gao, Z. Guo, R. Fang, G. Hu, S. Bai, F. Li, *J. Am. Chem. Soc.* 146 (2024) 7332–7340.
- [35] Q. Yi, Y. Lu, X. Sun, H. Zhang, H. Yu, C. Sun, *ACS Appl. Mater. Interfaces* 11 (2019) 46965–46972.
- [36] C. Wang, Z. Sun, L. Liu, H. Ni, Q. Hou, J. Fan, R. Yuan, M. Zheng, Q. Dong, *Energy Environ. Sci.* 16 (2023) 3098–3109.
- [37] M. Zhu, X. Zheng, L. Li, X. Zhu, Z. Huang, G. Wang, Y. Zhang, H. Liu, F. Yu, L. Wen, H.-K. Liu, S.-X. Dou, C. Wu, *Energy Storage Mater.* 48 (2022) 466–474.
- [38] J. Chen, Y. Peng, Y. Yin, M. Liu, Z. Fang, Y. Xie, B. Chen, Y. Cao, L. Xing, J. Huang, Y. Wang, X. Dong, Y. Xia, *Energy Environ. Sci.* 15 (2022) 3360–3368.

Graphical Abstract

The temperature-adaptive electrolyte with non-solvating PhOCF_3 is proposed. The dipole-dipole interactions between PhOCF_3 and solvents facilitate an anion-rich solvation structure, which is preserved at low temperatures and enables the electrolyte to achieve good electrochemical performance.



Declaration of interests

The authors declare that they have no known competing financial interests or personal relationships that could have appeared to influence the work reported in this paper.

The authors declare the following financial interests/personal relationships which may be considered as potential competing interests: